XLIII CILAMCE
21–25, November, 2022
FOZ DO IGUAÇU – PR – BRAZIL

Numerical Simulation of a Forged Inconel 718 Alloy Indentation Process

José Felipe de Aguiar e Silva[1], Artur Silva Pereira[2], Lucival Malcher[2 3]

[1]*Institute of Chemistry, University of Brasília, Zip-Code 70.910-900, Asa Norte, Brasília – DF, Brazil*
[2]*Department of Mechanical Engineering, University of Brasília, Zip-Code 70.910-900, Asa Norte, Brasília – DF, Brazil*
[3]*lucival.malcher@gmail.com*

Abstract.
This work proposes the numerical simulation, through the finite element method, of an indentation test in the forged Inconel 718 alloy. Hardness tests are performed on the alloy, under three levels of strength. At the same time, process simulations are carried out to determine the same print obtained experimentally. The effect of spring back and the possible use of the method in the parametric identification of hardening properties of the alloy are evaluated, when there are small volumes of materials for mechanical characterization.

Keywords: indentation process; inconel 718; FEM

1 Introduction

The uniaxial strength test and the Brinnel hardness test are widely used for providing material's property such as plasticity parameters. The uniaxial strength test tensions a specimen of material, controls the displacement, and register the load by a load cell. The Brinnel hardness test, on the other hand, consist of pressing a hard steel ball under a known load into the material of interest. In the industry, the most prioritized tests are the cheapest, the non-destructive and the ones that are directly applicable to products. Hence, this work focusses on numerical simulation of the Brinnel hardness test. Mathematically, the Brinell hardness H is given by the fraction of the load P by the surface area of the indentation (a spherical cap) [1], which was also proposed by Martens [2]:

$$H = \frac{P}{\pi D d}, \tag{1}$$

where D is the diameter of the spherical indenter and d is the depth of the indentation. In later works, Meyer [3] found out a relation between the load P and the diameter of de indentation d_i:

$$P = a d_n^i, \tag{2}$$

where a and n are numbers dependent on material's property. In addition, a depends on the sphere's size. Another point proposed by Meyer and validated by many authors ([4–6]) is described by the following equation:

$$H = \frac{P}{(\pi D/2)\left[D - (D^2 - d_i^2)\right]^{1/2}}, \tag{3}$$

which represents the load per indentation's projected area. In a nutshell, the method assays the crater load-depth left by the indenter, or yet the load-resultant area, also providing the Young's Modulus and Poisson's ratio. In addition, a recent Boutrid et. al paper [7] described a sequence of expressions for processing the data gained from a triaxial Brinell hardness test in some rocks in order to find their Young´s Modulus and the Poisson' ratio and the results were pretty satisfactory: the HB increases linearly with the Young's Modulus. The final equations used for the data treatment are the following:

$$E = \frac{\sigma_{z_2} - \sigma_{z_1}}{\xi_{z_2} - \xi_{z_1}}, \tag{4}$$

and

$$\upsilon = \frac{E\left(\xi_{z_2} - \xi_{z_1}\right)}{\sigma_{z_2} - \sigma_{z_1}}, \tag{5}$$

where the subscript informs the variation on deformation (ξ) and tension (σ) on the z axes from the initial (1) to the final (2) values.

However, both tensile and Brinell tests have an associated difficulty to them: the needed amount of material for performing the experiments, which in the first case is larger than the second. By the craving of solving this problem and optimizing the tests Machado and Malcher [8] applied Kleinermann-Ponhot constitutive model to SAE 1524 in FEM in order to provide the same results as the most real-life used tests. The method aims at an inverse analysis for obtaining the material's hardening parameters. Its efficiency lies on the optimization algorithm performance which needs a key information: the indentation profile. The equivalent von Misses stress is calculated by the following equation:

$$\sigma_{eq} = \frac{1}{\sqrt{2}}\left[\left(\sigma_{xx} - \sigma_{yy}\right)^2 + \left(\sigma_{xx} - \sigma_{zz}\right)^2 + \left(\sigma_{yy} - \sigma_{zz}\right)^2 + 6\left(\tau_{xy}^2 + \tau_{xz}^2 + \tau_{yz}^2\right)\right], \tag{6}$$

where σ_{xx}, σ_{yy}, σ_{zz}, τ_{xy}, τ_{xz} e τ_{yz} are the stress tensor components. In terms of plasticity, the point under de indenter amasses the hole plastic characteristic which is restricted by the elastic free surface until it achieves the yield stress, after this level of concentrated applied pressure, the plastic deformation immerges and the pressure is redistributed over the contact surface ([9, 10]). For a closer real-life and simulation relation certain parameters are determined such as compression time, applied force and diameter of the load-depth onto reliable data supply. This information allows the understanding of the behavior of a material and its ability to resist plastic deformation. Currently, the technology has provided sufficient tools to resolve numerous tasks and this test would be no different. Using numerical methods, as the Finite Elements Method (FEM), it is possible to simulate tests with high levels of accuracy, making this type of procedure very cheap and fast [8].

The forged Inconel 718, a polycristalline nickel-based superalloy, is known to be highly resistant to high temperatures and corrosion. This fact makes this material widely used in aviation and aerospace industry. Thus, scientists and engineers are constantly trying to implement this kind of alloy in order to improve the reliability and efficiency of engines, not to mention their balance between cost and performance. Some examples of usages of inconel 718 include turbine engines, cryogenic tankage and rocket fuel tank [12, International].

Now, applying this knowledge to a numerical method, it is possible to see a relationship between the stress-strain curve of the material and the indentation test. This methodology is innovative because it presents the inverse problem, in other words, it sets the stress-strain curve obtained from the experiment using the Inconel 718, in order to simulate the mechanical behavior of an indented material [8].

2 Methodology

For the simulation of the Brinell hardness test, the Abaqus CAE program was used. To start the project, the specimen was designed in the program as an axisymmetric Fig. 1a and 1b deformable solid, 5 mm wide and 5 mm high and the indenter as an axisymmetric rigid body, a semicircle with a radius of 1.25 mm. After setting the material properties and assigning them to the drawn parts, the indenter and the specimen are put together Fig. 1c so that forces can be applied. In addition, for the simulation works, three boundary conditions were placed: displacement, allowing the indenter to move only on the Y axis; encastre, preventing any movement of the specimen base; retraction, removing the contact between the indenter and the specimen after load application, allowing the observation of an elastic effect of material. Three forces were applied to the material: 31.25 kgf, 62.5 kgf and 187.5 kgf. For each one, a mesh convergence was made, which will be seen and discussed in the section results.

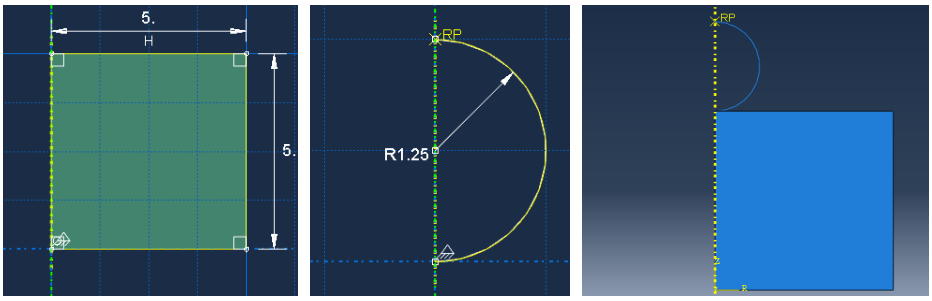

(a) designed specimen **(b)** designed indenter sphere **(c)** indenter placed on the specimen to enable the simulation

Figure 1 Sequence from designing to the assembled problem.

The material studied in this work, forged Inconel 718, was assigned to the specimen. The elastic properties used were as follows: a Young's Modulus of 185 GPa and a Poisson's Ratio of 0.33 [12]. Nevertheless, the determination of the behavior of material in plastic domain is very complex. Therefore, a non-linear mathematical model for material hardening was used, the Kleinermann and Ponthot's equation:

$$\sigma_y = \sigma_{y0} + \xi\overline{\varepsilon}_p + (\sigma_\infty - \sigma_{y0})\left(1 - e^{-\delta\overline{\varepsilon}_p}\right). \tag{7}$$

Three of the parameters used in eq. 7 are determined by numerical methods (ξ, σ_∞ and δ), as performed in this work, and the other one is the yield point (σ_{y0}). The yield tension described in this same equation, which varies with plastic strain ($\overline{\varepsilon}_p$), results in a stress-strain curve in the Fig. 2 that determines the plastic properties of the material.

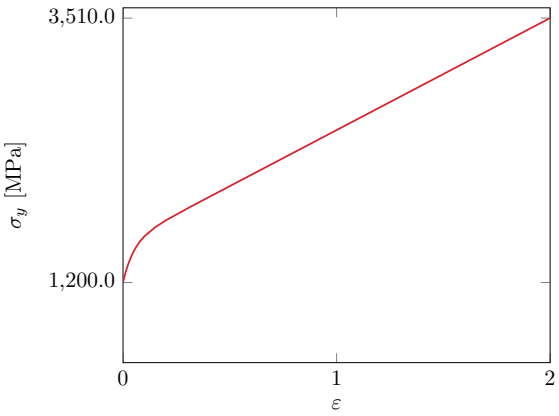

Figure 2 Stress-strain curve determined by the Kleinermann and Ponthot's equation.

3 Results

The main route to a good simulation is to know how to use a mesh correctly and optimize it, so that it represents reality as closely as possible and has the lowest possible computational cost. Thus, three mesh convergences were performed, one for each force applied to the specimen, in order to find the mesh size that best fits the previously established standards. For this, eight mesh sizes, linear and quadratic geometric order and quadratic elements were used. The simulation was divided into two steps. The first step refers to the application of the load on the specimen and the second step is the retraction of the indenter to observe the elastic effect of the material.

		Step 1			Step 2		
Force		187.5 kgf	62.5kgf	31.25 kgf	187.5 kgf	62.5kgf	31.25 kgf
Mesh size	Number of nodes	Displacement [mm]					
0.05	10223	0.0638132	0.0273969	0.0167798	0.0503698	0.0189824	0.0115097
0.07	5206	0.0637747	0.0262994	0.0168111	0.0496472	0.0185014	0.0112740
0.09	3271	0.0637353	0.0277217	0.0178792	0.0512168	0.0187881	0.0136394
0.11	2138	0.0616550	0.0280361	0.0175164	0.0478586	0.0216413	0.0129250
0.14	1391	0.0748793	0.0334338	0.0164850	0.0563975	0.0273034	0.0094675
0.17	992	0.0634055	0.0260201	0.0202495	0.0521857	0.0192214	0.0115293
0.20	698	0.0776042	0.0291548	0.0248772	0.0683657	0.0207601	0.0154089
0.25	463	0.0621695	0.0381483	0.0233633	0.0600477	0.0296083	0.0103053

Analyzing the results of mesh convergence, it is notable that the ones that had a smaller mesh size, consequently having a higher precision, had closer results between them. However, being more careful with the whole result, through the number of nodes and elements, it is noticed that they have a high computational cost in relation to other larger meshes performed. Creating a relationship between the number of nodes and the average displacement of the three forces applied and in step 1 (figure 3), it is possible to see that there is a certain convergence from 2138 nodes, but analyzing the whole scenario, it is noticed that the mesh of size 0.17 has results very close to the smallest mesh sizes, indicating that it is a good choice for the mesh, since it is not a coarse mesh, but it is also not too refined, so it will present results close to reality and with a lower computational cost. Analyzing beyond the average observed in figure 3, it is possible to observe the aforementioned behavior of this mesh individually in each mesh convergence performed.

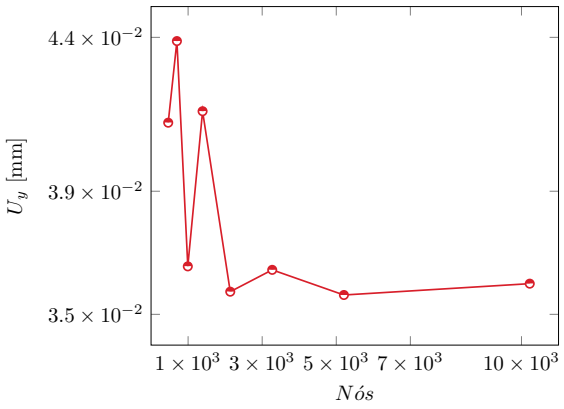

Figure 3 Gráfico que ilustra a curva de deslocamento pela quantidade de nós presentes no tamanho da malha.

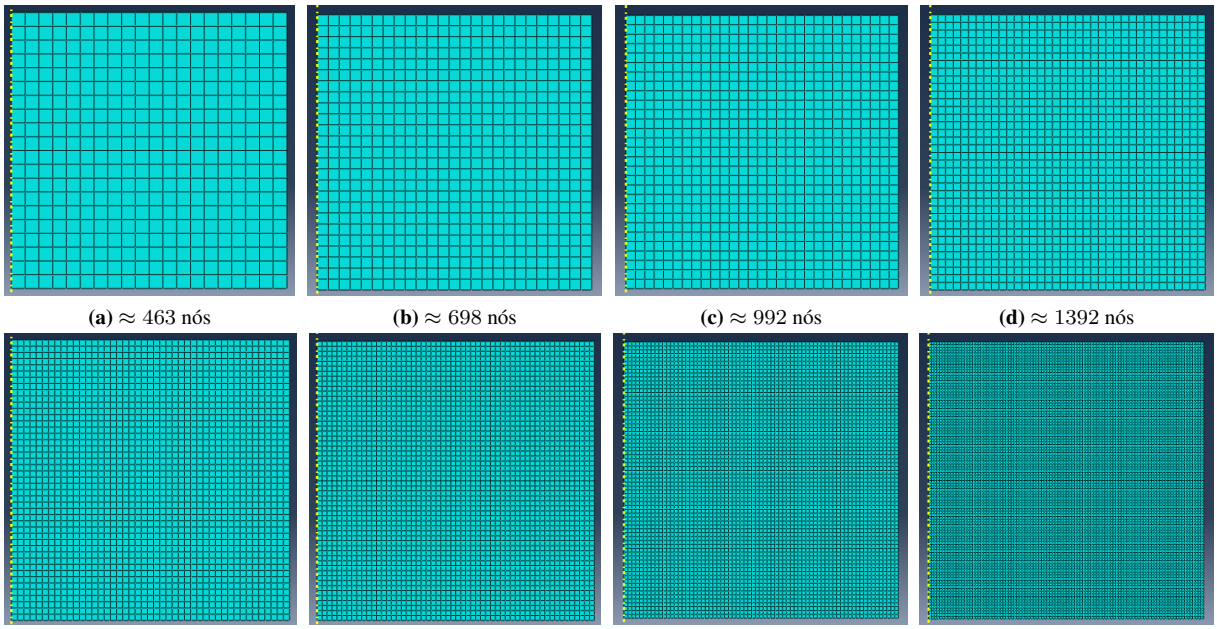

(a) $\approx$ 463 nós **(b)** $\approx$ 698 nós **(c)** $\approx$ 992 nós **(d)** $\approx$ 1392 nós

(e) $\approx$ 2138 nós **(f)** $\approx$ 3271 nós **(g)** $\approx$ 5206 nós **(h)** $\approx$ 10223 nós

Figure 4 mesh size of the specimen ($T_a = 0,25$ mm, $T_b = 0,20$ mm, $T_c = 0,17$ mm, $T_d = 0,14$ mm, $T_e = 0,11$ mm, $T_f = 0,09$ mm, $T_g = 0,07$ mm, $T_h = 0,05$ mm)

The mesh size 0.17 was chosen as a great candidate to serve as study parameters for this simulation. In addition, the indenter mesh was fixed and with a size of 0.2.

With the mesh ready, it is possible to run the program to verify the results obtained from the simulation and its elastic effects. Thus, applying the three forces scales was obtained the following results, as shown on the images above.

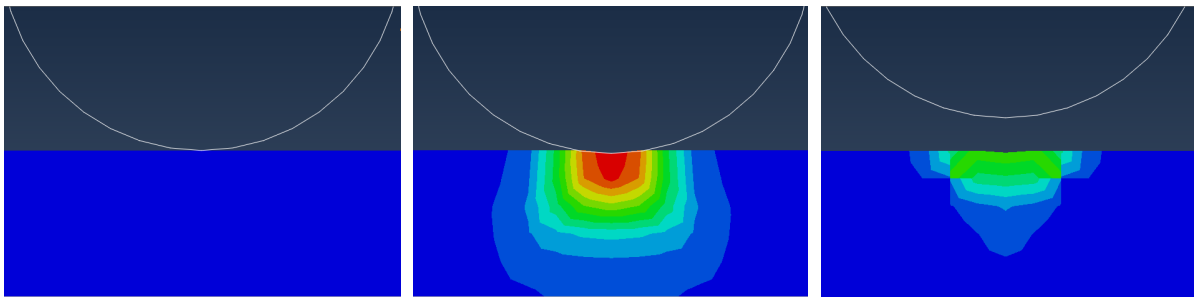

(a) start of indentation test **(b)** middle of indentation test **(c)** end of indentation test

Figure 5 test of the force of 31.25 kgf applied on the specimen

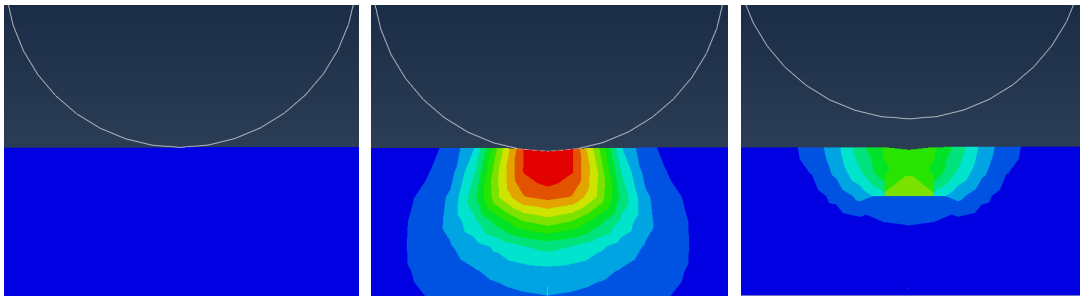

(a) start of indentation test **(b)** middle of indentation test **(c)** end of indentation test

Figure 6 test of the force of 62.5 kgf applied on the specimen

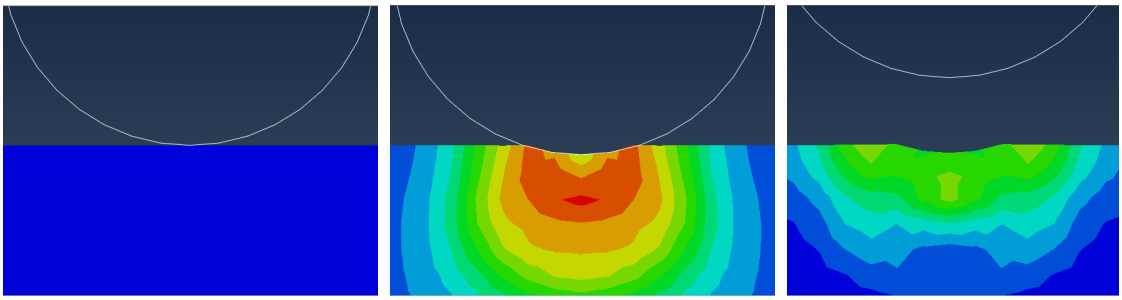

(a) start of indentation test **(b)** middle of indentation test **(c)** end of indentation test

Figure 7 test of the force of 187.5 kgf applied on the specimen

The first image of the sequence shows the process before its starts; the second represents step 1, with the indenter penetrating the specimen; the third one represents the final result, step 2, showing the effect of spring back. This process is observed in the three forces. As seen in the imagens from the simulation, all applied forces generated a depth-load, wich variated in size according to the magnitude used.

4 Conclusions

Through the steps carried out in this work, it is possible to verify that the numerical methods are of great value for the performance and optimization of damages tests, reducing manual wear and related costs. In addition, the finite element method is a great ally in the analysis of results, since it works through the inverse process. Thus, programming the simulations correctly, it is possible to observe several important parameters for a good application of the material studied and, thus, make its characterization of properties easier. This is explained in the spring back effect of the forged Inconel 718 shown in the passage from step 1 to step 2, when the indenter ceases to have contact with the specimen and begins to retract and, then, the material already with an accumulation of deformation has an elastic effect.

Acknowledgements. The authors are thankful to CAPES, CNPQ, DEG and the University of Brasília.

Authorship statement. The authors hereby confirm that they are the sole liable persons responsible for the authorship of this work, and that all material that has been herein included as part of the present paper is either the property (and authorship) of the authors, or has the permission of the owners to be included here.

References

[1] J. Springer. Methods of testing materials for hardness. *Cassier's Mag*, vol. 34, pp. 387–401, 1908.
[2] A. Martens. Handbuch der materialkunde, bd. 1 und 2, 1898.
[3] E. Meyer. *Untersuchungen über härteprüfung und härte*. Julius Springer, 1909.
[4] M. Meyer, L. VAN, and K. BLOK. Plastic deformation and the meyer constants of metals. *Nature*, vol. 169, n. 4293, pp. 237–238, 1952.
[5] A. Lankov. The meyer law and strain hardening of elastoplastic materials. *JOURNAL OF FRICTION AND WEAR C/C OF TRENIE I IZNOS*, vol. 14, pp. 18–18, 1993.
[6] M. Sakai. The meyer hardness: A measure for plasticity? *Journal of Materials Research*, vol. 14, n. 9, pp. 3630–3639, 1999.
[7] A. Boutrid, S. Bensehamdi, and R. Chaib. Investigation into brinell hardness test applied to rocks. *World Journal of Engineering*, 2013.
[8] L. Machado and L. Malcher. Isotropic hardening curve characterization by the resultant profile of ball indentation tests. *Journal of the Brazilian Society of Mechanical Sciences and Engineering*, vol. 41, n. 11, pp. 1–14, 2019.
[9] D. Hills. Some aspects of post-yield contact problems. *Wear*, vol. 85, n. 1, pp. 107–119, 1983.
[10] K. L. Johnson and L. M. Keer. Contact Mechanics. *Journal of Tribology*, vol. 108, n. 4, pp. 659–659, 1986.
[International] C. International. Inconel alloy 718: Properties and applications.
[12] B. Erice and F. Gálvez. A coupled elastoplastic-damage constitutive model with lode angle dependent failure criterion. *International Journal of Solids and Structures*, vol. 51, n. 1, pp. 93–110, 2014.